Nuclear Mathematical and Computational Sciences: A Century in Review, A Century Anew
Gatlinburg, Tennessee, April 6-11, 2003, on CD-ROM, American Nuclear Society, LaGrange Park, IL (2003)

CONSISTENT SPATIAL DISCRETIZATION OF THE LOW-ORDER QUASIDIFFUSION EQUATIONS ON COARSE GRIDS

Dmitriy Y. Anistratov
Department of Nuclear Engineering
North Carolina State University
Raleigh, NC 27695-7909
anistratov@ncsu.edu

ABSTRACT

In this paper we develop a spatial discretization method for the low-order quasidiffusion equations on coarse grids for full-core reactor calculations. The proposed method reproduces accurately the complicated large-scale behavior of the transport solution within assemblies. The resulting discretization is spatially consistent with a fine-mesh discretization of the transport equation in the sense that it preserves zeroth, first and second spatial Legendre moments of the fine-mesh transport solution over coarse-mesh cells along with the surface currents, and eigenvalue. Numerical results that demonstrate accuracy of the proposed methodology are presented.

Key Words: neutron transport, reactor physics calculations, coarse-mesh discretization

1. INTRODUCTION

The present computational methodologies for reactor analysis are based on full-core and assembly-level calculations. Full-core calculations generate eigenvalues and power distributions for a reactor core using few-group diffusion equation approximated on coarse grids. Each grid cell represents a large part of an assembly. The group data (i.e. cross sections, diffusion coefficients, discontinuity factors and other functionals) are obtained from assembly-level transport calculations in which the many-group transport equation is solved in isolated assembly with reflective boundary conditions on fine spatial grids.

An alternative approach was recently developed [1–6]. To account for the complicated transport effects in full-core calculations, a new methodology is based on low-order quasidiffusion (LOQD) equations [7–9]. This approach is also combined with single-assembly transport calculations that use special albedo boundary conditions which enable one to simulate efficiently effects of an unlike neighboring assembly on assembly's group data [2, 6].

The LOQD equations can capture transport effects to an arbitrary degree of accuracy. These equations can be reduced to a diffusion-like form. These features make the LOQD equations very attractive for using them as a background for methodology for reactor core calculations. In full reactor core calculations, it is necessary to use discretization methods that are very accurate on coarse meshes. In this paper we develop methods for approximating of the LOQD equations on coarse grids. It is necessary for such method to preserve the averaged reaction rates, surface-averaged group currents, and eigenvalue [10]. The way to improve accuracy of coarse-mesh calculations is to put more physics into coarse-mesh solution. This can be achieved by developing coarse-mesh discretization methods that reproduce accurately the large-scale behavior of the transport solution within assemblies that is characterized by a set of its pin-cell average values.

In this paper we present a finite-element discretization scheme of the low-order equations of the quasidiffusion (QD) method on coarse grids. On the basis of this scheme, we develop a coarse-mesh discretization of the LOQD equations that preserves exactly several spatial moments of the fine-mesh transport solution over coarse-mesh cells (e.g., assembly or quarter assembly). We analyze the behavior of the proposed method on numerical test problems that simulate the interaction of MOX and uranium assemblies with enrichment variations and water holes, and consider sensitivity of the coarse-mesh solution to perturbations in group data.

The reminder of the paper is organized as follows. In Sec. 2 we formulate the few-group LOQD equations. In Sec. 3 we derive a basic coarse-mesh finite element method for the LOQD equations that preserves zeroth moment of the fine-mesh transport solution as well as surface currents and eigenvalue. In Sec. 4 we present an advanced coarse-mesh finite-element method that preserves extra spatial moments of the fine-mesh transport solution. In Sec. 5 we demonstrate numerical solutions of test problems that simulate the interaction of MOX and uranium assemblies. We conclude with a discussion in Sec. 6.

2. THE FEW-GROUP LOW-ORDER QUASIDIFFUSION EQUATIONS

2.1 The LOQD Equations

We consider a few-group k-eigenvalue transport problem for 1D slab geometry with vacuum boundary conditions, $0 \le x \le X$, $g = 1, ..., M_g$. The LOQD equations [7, 9, 11, 12] for the group scalar flux ϕ^g and current J^g are

$$\frac{d}{dx} J^g + \Sigma_t^g \phi^g = \sum_{p=1}^{M_g} \Sigma_{s,0}^{p\to g} \phi^p + \frac{1}{k_{eff}} \chi^g \sum_{p=1}^{M_g} \nu_f^p \Sigma_f^p \phi^p \ , \tag{1}$$

$$\frac{d}{dx} \left(E^g \phi^g \right) + \Sigma_t^g J^g = 0 \ , \tag{2}$$

$$J^g(0) = C_L^g \phi^g(0) \ , \quad J^g(X) = C_R^g \phi^g(X) \ . \tag{3}$$

The functionals E^g, C_L^g and C_R^g are calculated by means of the few-group transport solution

$$E^g = \int_{-1}^{1} \mu^2 \psi^g d\mu \Big/ \int_{-1}^{1} \psi^g d\mu \ , \tag{4}$$

$$C_L^g = \int_{-1}^{0} \mu \psi^g d\mu \Big/ \int_{-1}^{0} \psi^g d\mu \Bigg|_{x=0} \ , \quad C_R^g = \int_{0}^{1} \mu \psi^g d\mu \Big/ \int_{0}^{1} \psi^g d\mu \Bigg|_{x=X} \tag{5}$$

where ψ^g is the group angular flux. The LOQD problem (1)-(3) exactly reproduces the transport scalar flux and current provided that the functionals are exact.

2.2 Generation of Few-Group Data

The LOQD equations are used in combination with assembly-level transport calculations that utilize the albedo boundary conditions without making color-set calculations, to simulate interaction with adjacent assembly in a reactor core.

Let us consider that each coarse-mesh cell represents a whole assembly. To generate fine-mesh transport solution for a given assembly (coarse cell) and calculate the averaged cross sections and functionals for the few-group coarse-mesh discretized LOQD equations, we perform a set of single-assembly fine-group transport calculations on fine spatial mesh with albedo boundary conditions ($0 \le x \le X$)

$$\psi^m(0,\mu) = \gamma_L^m(\mu)\psi^m(0,-\mu)\,,\ \text{for}\ \mu > 0\,, \quad \psi^m(X,\mu) = \gamma_R^m(\mu)\psi^m(X,-\mu)\,,\ \text{for}\ \mu < 0 \tag{6}$$

where γ_L^m, γ_R^m are albedos. The resulting boundary conditions for the fine-group LOQD equations have the following form:

$$J^m(0) = \frac{1-\lambda_{L,1}^m}{1+\lambda_{L,0}^m} C_L^m \phi^m(0)\,, \quad \lambda_{L,n}^m = \int_0^1 \mu^n \gamma_L^m(-\mu)\psi^m(0,\mu)d\mu \Big/ \int_0^1 \mu^n \psi^m(0,\mu)d\mu\,, \tag{7}$$

$$J^m(X) = \frac{1-\lambda_{R,1}^m}{1+\lambda_{R,0}^m} C_R^L \phi^m(X)\,, \quad \lambda_{R,n}^m = \int_{-1}^0 \mu^n \gamma_R^m(-\mu)\psi^m(X,\mu)d\mu \Big/ \int_{-1}^0 \mu^n \psi^m(X,\mu)d\mu\,, \tag{8}$$

where $n = 0, 1$. In this methodology various albedos are used to simulate interface phenomena between different assemblies [1, 2, 6].

2.3 Fine-Mesh Transport Solution

Assume that the reference fine-mesh transport solution of a given problem is known from calculations by means of some transport differencing method, and we have the fine-mesh transport solution defined by fine-mesh eigenvalue k_{eff}^{fm}, discrete grid functions of fine-mesh scalar flux $\phi_h^{g,fm}$, and current $J_h^{g,fm}$, which are defined as

$$J_h^{g,fm} = \{J_{i-1/2}^{g,fm}, i = 1, ..., N_x^{fm}+1\}\,, \tag{9}$$

$$\phi_h^{g,fm} = \{\phi_i^{g,fm}, i = 1, ..., N_x^{fm};\ \phi_{j-1/2}^{g,fm}, i = 1, ..., N_x^{fm}+1\}\,. \tag{10}$$

where the fine mesh is given by $\{x_{i-1/2}^{fm},\ i = 1, ..., N_x^{fm}+1,\ x_{1/2}^{fm} = 0,\ x_{N_x^{fm}+1/2}^{fm} = X\}$.

3. COARSE-MESH FINITE-ELEMENT DISCRETIZATION METHOD FOR THE LOQD EQUATIONS

Let us define the following coarse mesh $\{x_{j-1/2},\ j = 1, ..., N_x^{cm}+1\}$. The width of the jth coarse-mesh interval is $H_j = x_{j+1/2} - x_{j-1/2}$. The LOQD equations are approximated by means of a coarse-mesh finite-element (CMFE) method based on the following expansion of the coarse-mesh scalar flux

$$\Phi_j^g(x) = \sum_{l=0}^{2}(2l+1)\varphi_j^{(l),g} P_l(\zeta_j(x)) + \varphi_j^{(3),g}\sinh(\varkappa_j^g(x-x_j)) + \varphi_j^{(4),g}\cosh(\varkappa_j^g(x-x_j))\,, \tag{11}$$

where P_l are Legendre polynomials,

$$\zeta_j(x) = 2(x-x_j)/H_j\,, \quad x_j = 0.5(x_{j+1/2}+x_{j-1/2})\,, \quad 1 \le j \le N_x^{cm}\,, \tag{12}$$

and

$$\varkappa_j^g = \sqrt{(\langle\Sigma_t\rangle_j^g - \langle\Sigma_{s,0}\rangle_j^{g\to g})\langle\Sigma_t\rangle_j^g \Big/ \langle E\rangle_j^g}\,. \tag{13}$$

Note that we use brackets $\langle\bullet\rangle$ for quantities spatially averaged over coarse cells and defined as

$$\langle\mathcal{A}\rangle_j^g = \sum_{i\in\omega_j}\mathcal{A}_i^g\phi_i^{g,fm}h_i \Big/ \sum_{i\in\omega_j}\phi_i^{g,fm}h_i\,, \tag{14}$$

where

$$\omega_j = \{i : x_{j-1/2} \le x_{i-1/2}^{fm} < x_{j+1/2}\} \tag{15}$$

is a set of indices of fine-mesh cells that belong to the jth coarse-mesh cell, $h_i = x_{i+1/2}^{fm} - x_{i-1/2}^{fm}$ is the width of the ith fine-mesh cell.

To derive a scheme for the LOQD equations, we integrate the balance equation (1) with weights $P_l(\zeta_j(x))$ $l = 0, 1, 2$ over coarse interval $x_{j-1/2} \le x \le x_{j+1/2}$. Using Eq.(2), we get the following set of coarse-cell spatial moments of the balance equation:

$$J_{j+1/2}^g - J_{j-1/2}^g + \langle\Sigma_t\rangle_j^g H_j\Phi_j^{(0),g} = H_j\sum_{p=1}^{M_g}\langle\Sigma_{s,0}\rangle_j^{p\to g}\Phi_j^{(0),p} + \frac{H_j}{k_{eff}}\sum_{p=1}^{M_g}\langle\chi\nu_f\Sigma_f\rangle_j^{p,g}\Phi_j^{(0),p}\,, \tag{16}$$

$$J_{j+1/2}^g + J_{j-1/2}^g + \frac{2}{\langle\Sigma_t\rangle_j^g H_j}\left(\{E\}_j^{g,+}\Phi_j^g(x_{j+1/2}) - \{E\}_j^{g,-}\Phi_j^g(x_{j-1/2})\right) + \langle\Sigma_t\rangle_j^g H_j\Phi_j^{(1),g} = \tag{17}$$

$$H_j\sum_{p=1}^{M_g}\langle\Sigma_{s,0}\rangle_j^{p\to g}\Phi_j^{(1),p} + \frac{H_j}{k_{eff}}\sum_{p=1}^{M_g}\langle\chi\nu_f\Sigma_f\rangle_j^{p,g}\Phi_j^{(1),p}\,,$$

$$J_{j+1/2}^g - J_{j-1/2}^g + \frac{6}{\langle\Sigma_t\rangle_j^g H_j}\left(\{E\}_j^{g,+}\Phi_j^g(x_{j+1/2}) + \{E\}_j^{g,-}\Phi_j^g(x_{j-1/2}) - 2\langle E\rangle_j^g\Phi_j^{(0),g}\right) + \langle\Sigma_t\rangle_j^g H_j\Phi_j^{(2),g} = \tag{18}$$

$$H_j\sum_{p=1}^{M_g}\langle\Sigma_{s,0}\rangle_j^{p\to g}\Phi_j^{(2),p} + \frac{H_j}{k_{eff}}\sum_{p=1}^{M_g}\langle\chi\nu_f\Sigma_f\rangle_j^{p,g}\Phi_j^{(2),p}\,,$$

where

$$\Phi_j^{(l),g} = \frac{1}{H_j}\int_{x_{j-1/2}}^{x_{j+1/2}} P_l(\zeta_j(x))\Phi_j^g(x)dx\,, \quad l = 0, 1, 2 \tag{19}$$

are spatial moments of the coarse-mesh scalar flux. The definitions of $\{E\}_j^{g,-}$ and$\{E\}_j^{g,+}$ are given below.

On the basis of Eq. (2), we formulate the relationship between the current, scalar flux and its derivative at the coarse-cell edges

$$\{E\}_j^{g,-}\left.\frac{d\Phi_j^g}{dx}\right|_{x=x_{j-1/2}} + \left\{\frac{dE}{dx}\right\}_j^{g,-}\Phi_j^g(x_{j-1/2}) + \{\Sigma_t\}_j^{g,-}J_{j-1/2}^g = 0\,, \tag{20}$$

$$\{E\}_j^{g,+}\left.\frac{d\Phi_j^g}{dx}\right|_{x=x_{j+1/2}} + \left\{\frac{dE}{dx}\right\}_j^{g,+}\Phi_j^g(x_{j+1/2}) + \{\Sigma_t\}_j^{g,+}J_{j+1/2}^g = 0\,. \tag{21}$$

The coefficients of these equations are calculated by means of pin-cell average data. Such quantities are denoted by $\{\bullet\}$. Assume that there are Z_j pin cells in the jth coarse interval. We define the pin-cell averaged quantities of the following form:

$$\{\mathcal{A}\}_j^{g,pin\#m} = \sum_{i\in\omega_j^{pin\#m}} \mathcal{A}_i^g \phi_i^{g,fm} h_i \Big/ \sum_{i\in\omega_j^{pin\#m}} \phi_i^{g,fm} h_i \,, \tag{22}$$

where $\omega_j^{pin\#m}$ is a set of indices of fine-mesh intervals that belong to the mth pin cell. In Eqs. (17)-(21) the functional E^g and total cross section are averaged over boundary pin cells

$$\{E\}_j^{g,-} = \{E\}_j^{g,pin\#1}\,,\ \{E\}_j^{g,+} = \{E\}_j^{g,pin\#Z_j}\,,\ \{\Sigma_t\}_j^{g,-} = \{\Sigma_t\}_j^{g,pin\#1}\,,\ \{\Sigma_t\}_j^{g,+} = \{\Sigma_t\}_j^{g,pin\#Z_j}\,, \tag{23}$$

and

$$\left\{\frac{dE}{dx}\right\}_j^{g,-} = 2\left(\{E\}_j^{g,pin\#2} - \{E\}_j^{g,pin\#1}\right)\Big/\left(H_j^{pin\#2} + H_j^{pin\#1}\right)\,, \tag{24}$$

$$\left\{\frac{dE}{dx}\right\}_j^{g,+} = 2\left(\{E\}_j^{g,pin\#Z_j} - \{E\}_j^{g,pin\#Z_j-1}\right)\Big/\left(H_j^{pin\#Z_j} + H_j^{pin\#Z_j-1}\right)\,, \tag{25}$$

where $H_j^{pin\#m}$ is the width of the mth pin cell. The equations (20) and (21) with group data defined by (23)-(25) enable us to approximate the large-scale behavior of the transport solution next to boundaries of coarse intervals. Note that the homogenization algorithms developed by Kord Smith [14] use group data that is averaged over boundary pin cells.

To complete the system of discretized equations of the proposed method, we define the discontinuity conditions for the scalar flux

$$G_j^{g,+}\Phi_j^g(x_{j+1/2}) = G_{j+1}^{g,-}\Phi_{j+1}^g(x_{j+1/2})\,,\quad j = 1,...,N_x^{cm}-1\,, \tag{26}$$

and boundary conditions (3)

$$J_{1/2}^g = C_L^g G_1^{g,-}\Phi_1^g(x_{1/2})\,,\quad J_{N_x^{cm}+1/2}^g = C_R^g G_{N_x^{cm}}^{g,+}\Phi_{N_x^{cm}}^g(x_{N_x^{cm}+1/2})\,. \tag{27}$$

As a result the coarse-mesh discretization method consists of the spatial moment equations (16)-(18), equations (20) and (21) at the edges of coarse cells, the discontinuity conditions (26), and the QD boundary conditions (27). Substituting the expansion (11) into these equations, one obtains the final set of algebraic equations for $\varphi_j^{(l),g}$, $l = 0,...,4$, $j = 1,...,N_x^{cm}$ and $J_{j-1/2}^g$, $j = 1,...,N_x^{cm}+1$, ($g = 1,...,M_g$).

The discontinuity factors are defined as the ratio

$$G_j^{g,\pm} = \phi_h^{g,fm}(x_{j\pm1/2}) \Big/ \tilde{\Phi}_j^g(x_{j\pm1/2})\,. \tag{28}$$

where $\phi_h^{g,fm}(x_{j\pm1/2})$ is the fine-mesh transport scalar flux at $x = x_{j\pm1/2}$. Here we utilize an auxiliary function $\tilde{\Phi}_j^g(x)$

$$\tilde{\Phi}_j^g(x) = \sum_{l=0}^{2}(2l+1)\tilde{\varphi}_j^{(l),g}P_l(\zeta_j(x)) + \tilde{\varphi}_j^{(3),g}\sinh(\varkappa_j^g(x-x_j)) + \tilde{\varphi}_j^{(4),g}\cosh(\varkappa_j^g(x-x_j)) \tag{29}$$

which is the solution of Eqs. (17)-(21) in each jth coarse cell provided that the cell-edge currents, cell average scalar flux, and eigenvalue equal to their fine-mesh values.

The coarse-mesh discrete LOQD equations (16)-(18), (20)-(21), (26) and (27) are consistent with the given transport differencing method that generates the reference numerical transport solution $\phi_h^{g,fm}$ and $J_h^{g,fm}$ in the sense that the coarse-mesh solution $\Phi_j^g(x)$ preserves the average value of the fine-mesh scalar flux and reaction rates over each coarse-mesh cell, fine-mesh currents on edges of coarse cells, and fine-mesh k-eigenvalue, i.e.

$$\Phi_j^{(0),g} = \frac{1}{H_j}\sum_{i\in\omega_j}\phi_i^{fm}h_i\,, \tag{30}$$

$$k = k^{fm}\,, \tag{31}$$

$$J_{j-1/2}^g = J_h^{g,fm}(x_{j-1/2})\,,\quad J_{j+1/2}^g = J_h^{g,fm}(x_{j+1/2})\,, \tag{32}$$

$$\langle\Sigma_t\rangle_j^g H_j\Phi_j^{(0),g} = \sum_{i\in\omega_j}\Sigma_{t,i}^g\phi_i^{g,fm}h_i\,,\quad \langle\Sigma_{s,0}\rangle_j^{p\to g}\Phi_j^{(0),p}H_j = \sum_{i\in\omega_j}\Sigma_i^{p\to g}\phi_i^{p,fm}h_i\,, \tag{33}$$

$$\langle\chi\nu_f\Sigma_f\rangle_j^{p,g}\Phi_j^{(0),p}H_j = \sum_{i\in\omega_j}\chi_i^g\nu_{f,i}^p\Sigma_{i,f}^p\phi_i^{p,fm}h_i\,. \tag{34}$$

Note that in terms of spatial moments of the scalar flux, the resulting coarse-mesh finite-element method (16)-(18), (20)-(21), (26) and (27) preserves only zeroth moment of fine-mesh transport solution. Hereafter we refer to this method as CMFE-0, where the number indicates the maximum order of the spatial moment of the fine-mesh transport solution preserved by the method.

4. ADVANCED CONSISTENT COARSE-MESH DISCRETIZATION

We now develop an advanced consistent coarse-mesh discretization method that preserves extra spatial moments of the fine-mesh transport solution, namely, first and second spatial Legendre moments of the fine-mesh scalar flux over each coarse cell,

$$\Phi_j^{(l),g} = \phi_j^{(l),g,fm}\,,\quad l = 1,2\,, \tag{35}$$

where

$$\phi_j^{(l),g,fm} = \frac{1}{H_j}\sum_{i\in\omega_j}\bar{\mathcal{P}}_i^{l,j}\phi_i^{g,fm}h_i \tag{36}$$

is the discrete form of spatial Legendre moments of the fine-mesh scalar flux over $x_{j-1/2}\le x\le x_{j+1/2}$, and

$$\bar{\mathcal{P}}_i^{l,j} = \frac{1}{h_i}\int_{x_{i-1/2}^{fm}}^{x_{i+1/2}^{fm}} P_l(\zeta_j(x))dx\,. \tag{37}$$

To formulate a scheme with the desired properties, we use the above method as a basis and add special consistency terms in the first and second spatial moments on the balance equations. The proposed CMFE

method is defined by

$$J^g_{j+1/2} - J^g_{j-1/2} + \langle \Sigma_t \rangle^g_j H_j \Phi^{(0),g}_j = H_j \sum_{p=1}^{M_g} \langle \Sigma_{s,0} \rangle^{p\to g}_j \Phi^{(0),p}_j + \frac{H_j}{k_{eff}} \sum_{p=1}^{M_g} \langle \chi \nu_f \Sigma_f \rangle^{p,g}_j \Phi^{(0),p}_j \,, \tag{38}$$

$$J^g_{j+1/2} + J^g_{j-1/2} + \frac{2}{\langle \Sigma_t \rangle^g_j H_j} \left(\{E\}^{g,+}_j \Phi^g_j(x_{j+1/2}) - \{E\}^{g,-}_j \Phi^g_j(x_{j-1/2}) \right) +$$

$$\langle \Sigma_t \rangle^g_j H_j \Phi^{(1),g}_j + \left(\alpha^{(1),g}_j + \beta^{(1),g}_{t,j} \right) H_j \Phi^{(0),g}_j = \tag{39}$$

$$H_j \sum_{p=1}^{M_g} \langle \Sigma_{s,0} \rangle^{p\to g}_j \Phi^{(1),p}_j + \frac{H_j}{k_{eff}} \sum_{p=1}^{M_g} \langle \chi \nu_f \Sigma_f \rangle^{p,g}_j \Phi^{(1),p}_j + H_j \sum_{p=1}^{M_g} \left(\beta^{(1),p\to g}_{s,j} + \frac{1}{k_{eff}} \beta^{(1),p,g}_{f,j} \right) \Phi^{(0),p}_j \,,$$

$$J^g_{j+1/2} - J^g_{j-1/2} + \frac{6}{\langle \Sigma_t \rangle^g_j H_j} \left(\{E\}^{g,+}_j \Phi^g_j(x_{j+1/2}) + \{E\}^{g,-}_j \Phi^g_j(x_{j-1/2}) - 2\langle E \rangle^g_j \Phi^{(0),g}_j \right) +$$

$$\langle \Sigma_t \rangle^g_j H_j \Phi^{(2),g}_j + \left(\alpha^{(2),g}_j + \beta^{(2),g}_{t,j} \right) H_j \Phi^{(0),g}_j = \tag{40}$$

$$H_j \sum_{p=1}^{M_g} \langle \Sigma_{s,0} \rangle^{p\to g}_j \Phi^{(2),p}_j + \frac{H_j}{k_{eff}} + \sum_{p=1}^{M_g} \langle \chi \nu_f \Sigma_f \rangle^{p,g}_j \Phi^{(2),p}_j H_j \sum_{p=1}^{M_g} \left(\beta^{(2),p\to g}_{s,j} + \frac{1}{k_{eff}} \beta^{(2),p,g}_{f,j} \right) \Phi^{(0),p}_j \,,$$

$$\{E\}^{g,-}_j \left. \frac{d\Phi^g_j}{dx} \right|_{x=x_{j-1/2}} + \left\{ \frac{dE}{dx} \right\}^{g,-}_j \Phi^g_j(x_{j-1/2}) + \{\Sigma_t\}^{g,-}_j J^g_{j-1/2} = 0 \,, \tag{41}$$

$$\{E\}^{g,+}_j \left. \frac{d\Phi^g_j}{dx} \right|_{x=x_{j+1/2}} + \left\{ \frac{dE}{dx} \right\}^{g,+}_j \Phi^g_j(x_{j+1/2}) + \{\Sigma_t\}^{g,+}_j J^g_{j+1/2} = 0 \,. \tag{42}$$

$$\widehat{G}^{g,+}_j \Phi^g_j(x_{j+1/2}) = \widehat{G}^{g,-}_{j+1} \Phi^g_{j+1}(x_{j+1/2}) \,, \quad j = 1, ..., N^{cm}_x - 1 \,, \tag{43}$$

$$J^g_{1/2} = C^g_L \widehat{G}^{g,-}_1 \Phi^g_1(x_{1/2}) \,, \quad J^g_{N^{cm}_x+1/2} = C^g_R \widehat{G}^{g,+}_{N^{cm}_x} \Phi^g_{N^{cm}_x}(x_{N^{cm}_x+1/2}) \,. \tag{44}$$

Here we use new discontinuity factors $\widehat{G}^{g,\pm}$ that are determined by means of different auxiliary function compared to one used to calculate $G^{g,\pm}$ in the CMFE-0 method.

The $\alpha^{(l),g}_j$, $\beta^{(l),g}_{t,j}$, $\beta^{(l),p\to g}_{s,j}$ and $\beta^{(l),p,g}_{f,j}$ are consistency terms that are defined such that the resulting scheme preserves: (i) fine-mesh values of the transport currents at edges of coarse cells, (ii) zeroth, first and second spatial Legendre moments of the fine-mesh transport scalar flux over each coarse cell. To derive such terms and get spatial moments equations consistent with the fine-mesh discretization scheme, we performed the operation of taking spatial moments of the balance equation (1) in discrete form by multiplying the fine-mesh discretized balance equation by $\bar{P}^{l,j}_i$ l=1,2, (Eq.(37)) and summing it over all fine-mesh cells that belong to the jth coarse interval

$$\sum_{i\in\omega_j} \bar{\mathcal{P}}^{l,j}_i \left(J^{g,fm}_{i+1/2} - J^{g,fm}_{i-1/2} \right) + \sum_{i\in\omega_j} \bar{\mathcal{P}}^{l,j}_i \Sigma^g_{t,i} \phi^{g,fm}_i h_i =$$

$$\sum_{p=1}^{M_g} \sum_{i\in\omega_j} \bar{\mathcal{P}}^{l,j}_i \Sigma^{p\to g}_{s,0,i} \phi^{p,fm}_i h_i + \frac{1}{k_{eff}} \sum_{p=1}^{M_g} \sum_{i\in\omega_j} \bar{\mathcal{P}}^{l,j}_i \chi^g_i \nu^p_{f,i} \Sigma^p_{f,i} \phi^{p,fm}_i h_i \,, \tag{45}$$

$$j = 1, ..., N_x^{cm} .$$

As a result we define the following functionals:

$$\alpha_j^{(1),g} = \left[\sum_{i\in\omega_j} \bar{\mathcal{P}}_i^{1,j} \left(J_{i+1/2}^{g,fm} - J_{i-1/2}^{g,fm} \right) - J_h^{g,fm}(x_{j+1/2}) - J_h^{g,fm}(x_{j-1/2}) - \right.$$

$$\left. \frac{2}{\langle\Sigma_t\rangle_j^g H_j} \left(\{E\}_j^{g,+} \frac{\phi_h^{g,fm}(x_{j+1/2})}{\widehat{G}_j^{g,+}} - \{E\}_j^{g,-} \frac{\phi_h^{g,fm}(x_{j-1/2})}{\widehat{G}_j^{g,-}} \right) \right] \Bigg/ \sum_{i\in\omega_j} \phi_i^{g,fm} h_i \,, \tag{46}$$

$$\alpha_j^{(2),g} = \left[\sum_{i\in\omega_j} \bar{\mathcal{P}}_i^{2,j} \left(J_{i+1/2}^{g,fm} - J_{i-1/2}^{g,fm} \right) - J_h^{g,fm}(x_{j+1/2}) + J_h^{g,fm}(x_{j-1/2}) - \right.$$

$$\left. \frac{6}{\langle\Sigma_t\rangle_j^g H_j} \left(\{E\}_j^{g,+} \frac{\phi_h^{g,fm}(x_{j+1/2})}{\widehat{G}_j^{g,+}} + \{E\}_j^{g,-} \frac{\phi_h^{g,fm}(x_{j-1/2})}{\widehat{G}_j^{g,-}} - 2\langle E\rangle_j^g \phi_j^{(0),g,fm} \right) \right] \Bigg/ \sum_{i\in\omega_j} \phi_i^{g,fm} h_i \,, \tag{47}$$

$$\beta_{t,j}^{(l),g} = \sum_{i\in\omega_j} \left[\Sigma_{t,i}^g - \langle\Sigma_t\rangle_j^g \right] \bar{\mathcal{P}}_i^{l,j} \phi_i^{g,fm} h_i \Bigg/ \sum_{i\in\omega_j} \phi_i^{g,fm} h_i \,, \tag{48}$$

$$\beta_{s,j}^{(l),p\to g} = \sum_{i\in\omega_j} \left[\Sigma_{s,0,i}^{p\to g} - \langle\Sigma_{s,0}\rangle_j^{p\to g} \right] \bar{\mathcal{P}}_i^{l,j} \phi_i^{p,fm} h_i \Bigg/ \sum_{i\in\omega_j} \phi_i^{p,fm} h_i \,, \tag{49}$$

$$\beta_{f,j}^{(l),p,g} = \sum_{i\in\omega_j} \left[\chi_i^g \nu_{f,i}^p \Sigma_{f,i}^p - \langle\chi\nu_f\Sigma_f\rangle_j^{p,g} \right] \bar{\mathcal{P}}_i^{l,j} \phi_i^{p,fm} h_i \Bigg/ \sum_{i\in\omega_j} \phi_i^{p,fm} h_i \,, \tag{50}$$

$$l = 1, 2 \,.$$

Note that we assumed that the discontinuity factors are known.

To define the discontinuity factors $\widehat{G}_j^{g,\pm}$, we use an auxiliary function

$$\widehat{\Phi}_j^g(x) = \sum_{l=0}^{2} (2l+1) \widehat{\varphi}_j^{(l),g} P_l(\zeta_j(x)) + \widehat{\varphi}_j^{(3),g} \sinh(\varkappa_j^g (x - x_j)) + \widehat{\varphi}_j^{(4),g} \cosh(\varkappa_j^g (x - x_j)) \tag{51}$$

which is the solution of Eqs. (38)-(44) for the jth coarse cell such that it reproduces the average value of the fine-mesh transport scalar flux, the first and second spatial Legendre moments of the fine-mesh transport scalar flux, and currents on edges of this coarse cell. To calculate the coefficients of expansion of $\widehat{\Phi}_j^g(x)$, we need to solve the following set of equations in terms of $\widehat{\varphi}_j^{(l),g}$, $l = 0, ..., 4$ in the jth cell:

$$\{E\}_j^{g,-} \left. \frac{d\widehat{\Phi}_j^g}{dx} \right|_{x=x_{j-1/2}} + \left\{ \frac{dE}{dx} \right\}_j^{g,=} \widehat{\Phi}_j^g(x_{j-1/2}) = -\{\Sigma_t\}_j^{g,-} J_h^{g,fm}(x_{j-1/2}) \,, \tag{52}$$

$$\{E\}_j^{g,+} \left. \frac{d\widehat{\Phi}_j^g}{dx} \right|_{x=x_{j+1/2}} + \left\{ \frac{dE}{dx} \right\}_j^{g,+} \widehat{\Phi}_j^g(x_{j+1/2}) = -\{\Sigma_t\}_j^{g,+} J_h^{g,fm}(x_{j+1/2}) \,, \tag{53}$$

$$\widehat{\Phi}_j^{(l),g} = \phi_j^{(l),g,fm} \,, \quad l = 0, 1, 2 \,. \tag{54}$$

The discontinuity factors are defined as the ratio

$$\widehat{G}_j^{g,\pm} = \phi_h^{g,fm}(x_{j\pm1/2}) \Big/ \widehat{\Phi}_j^g(x_{j\pm1/2}) \,. \tag{55}$$

The following theorem is true for the derived advanced consistent coarse-mesh discretization method:

Theorem *The coarse-mesh discrete low-order QD equations (38)-(44), with discontinuity factors (55), cross sections and functionals defined by (14), (23)-(25) and (46)-(50) are consistent with the given transport differencing method that generates the reference fine-mesh transport solution $\phi_h^{g,fm}$ and $J_h^{g,fm}$ in the sense that the coarse-mesh solution $\Phi_j^g(x)$ preserves the average value of the fine-mesh scalar flux and reaction rates over each coarse-mesh cell, the first and second spatial Legendre moments of the fine-mesh scalar flux over coarse intervals, fine-mesh currents at edges of coarse cells, and fine-mesh k-eigenvalue, i.e.*

$$\Phi_j^{(l),g} = \phi_j^{(l),g,fm} \,, \quad l = 0,1,2 \,, \quad J_{j\pm1/2}^g = J_h^{g,fm}(x_{j\pm1/2}) \,, \quad k_{eff} = k_{eff}^{fm} \,, \tag{56}$$

$$\langle \Sigma_t \rangle_j^g H_j \Phi_j^{(0),g} = \sum_{i\in\omega_j} \Sigma_{t,i}^g \phi_i^{g,fm} h_i \;, \quad \langle \Sigma_{s,0} \rangle_j^{p\to g} H_j \Phi_j^{(0),p} = \sum_{i\in\omega_j} \Sigma_{s,0,i}^{p\to g} \phi_i^{p,fm} h_i \;, \tag{57}$$

$$\langle \chi \nu_f \Sigma_f \rangle_j^{p,g} H_j \Phi_j^{(0),p} = \sum_{i\in\omega_j} \chi_i^g \nu_{f,i}^p \Sigma_{f,i}^p \phi_i^{p,fm} h_i \;. \tag{58}$$

Thus, the resulting coarse-mesh finite-element method preserves up to the second Legendre spatial moment of the fine-mesh transport scalar flux over coarse-cells. We refer to this method as CMFE-2.

5. NUMERICAL RESULTS

5.1 Test Problems that Simulate the Interaction of MOX and Uranium Assemblies

We present numerical results of Kord Smith's test problems in 1D slab geometry with two energy groups [14]. In these test problems, model uranium and MOX assemblies are used. There are two half-assemblies next to each other with reflective boundary conditions on the outside. A MOX half-assembly is on the left and a uranium half-assembly is on the right. Each half-assembly consists of 8 pin cells. A fuel pin cell is 1.25 cm wide with fuel pin (0.625 cm) located in its center and surrounded by water. The half-assembly width is 10 cm. Table I shows cross sections of different types of fuels and water. Figures 1-5 demonstrate design of assemblies for each test problem. Test 1 and 2 consists of assemblies with the same type of fuel pins. Test 3 and 4 differ from Test 2 by design of MOX assemblies. These tests simulate variation in enrichment near the interface with a uranium assembly. Test 5 has a MOX assembly with a water hole.

The fine-mesh solutions were calculated by the QD method using a second order finite-volume scheme for the LOQD equations and step characteristic method for the transport equation to calculate the QD functionals [13]. The fine spatial mesh consists of 128 equal cells, i.e. 8 mesh cells per pin cell. The angular mesh has 10 intervals. The multiplication factor equals 1.5. The coarse mesh consists of one cell per half-assembly; thus, $N_x^{cm} = 2$.

Figures 6-15 show the fine-mesh transport scalar fluxes versus position, pin-cell average values of the scalar flux represented as a histogram plot, and coarse-mesh solutions obtained by means of the CMFE-0

and CMFE-2 methods. Tables II-XI present the relative difference in pin-cell average values of the fine-mesh transport solution and coarse-mesh LOQD solution calculated by the CMFE-0 and CMFE-2 methods. In each assembly pin cells are numbered from left to right. The largest absolute values of relative differences in pin-cell average values of the fine-mesh transport solution and coarse-mesh LOQD solution in MOX assemblies are listed in Table XII.

The results of Tests 1 an 2 demonstrate that both methods generate very accurate coarse-mesh solutions, if assemblies consist of the same type of fuel pins. In Tests 3 and 4 that simulate spatial variation of fuel enrichment in MOX assembly, the CMFE-2 method approximates accurately the large-scale behavior of the transport solution characterized by the pin-cell average values. The resulting coarse-mesh solution of the CMFE-2 is significantly more accurate compared to the coarse-mesh solution obtained by the CMFE-0 method that preserves only zeroth spatial moment of the scalar flux. In Test 5 with the water hole in the MOX assembly the CMFE-2 method mimics the large-scale behavior of the fine-mesh transport solution and generates coarse-mesh solution with sufficiently good accuracy. These results demonstrate that the preservation of extra spatial moments of the fine-mesh transport solution leads to significant improvement in accuracy of the coarse-mesh solution.

5.2 Stability of Consistent Discretization to Variation of Group Data

In calculations of the presented test problems, all necessary assembly-averaged cross sections and functionals (discontinuity factors, quasidiffusion functionals, consistency terms, etc.) were exact, because they were generated by means of fine-mesh transport solutions of corresponding coupled assemblies. In terms of the methodology for full-core calculations described above, this means that exact albedos were used in single-assembly calculations to generate assembly group data. However, in realistic calculations the assembly group data are arranged in form of tables, and necessary quantities are determined by means of interpolation of tabulated data. Thus, it is interesting to study the stability of solution obtained by means of CMFE-2 to variation in cross sections and functionals of this method, to find out how this can influence the accuracy of the coarse-mesh solution generated by CMFE-2.

To perform this kind of analysis, we calculated Test 3 with the group data for the MOX assembly obtained by using perturbed averaging function. The group data were obtained by means of transport solutions of two assembly problems similar to Test 3 but in which the neighboring uranium assembly had perturbed σ_f^2 (Test 6) or ν_f^2 (Tests 7), namely, decreased by 5% and 10%. Figures 16-19 show the results of Tests 6 and 7.

From these results we notice that the obtained solutions in each case is very close to the solution of Test 3 in which exact group data were used. Thus, the proposed advanced consistent coarse-mesh discretization method, CMFE-2, demonstrates stability to variation in averaging function that is used for calculating group data, and, as a result, to variation in group data.

6. CONCLUSIONS

We have presented a high-order coarse-mesh finite-element (CMFE-0) method for discretization of the QD low-order equations that is consistent with the given fine-mesh transport differencing method in the sense that it preserves the fine-mesh values of cell-average scalar flux, cell-edge current, multiplication factor, and reaction rates. On the basis of this method, we have developed an advanced consistent coarse-mesh finite-element (CMFE-2) method that preserves extra two spatial Legendre moments of the fine-mesh transport scalar flux over coarse-mesh cells.

Table I. Cross Sections Data

Notation	Material	Σ_t^1	$\Sigma_{s,0}^{1\to1}$	$\Sigma_{s,0}^{1\to2}$	Σ_f^1	ν_f^1	Σ_t^2	$\Sigma_{s,0}^{2\to2}$	$\Sigma_{s,0}^{2\to1}$	Σ_f^2	ν_f^2
M1	MOX fuel	0.2	0.2	0	0	0	0.6	0	0	0.6	1.5
M2	MOX fuel	0.2	0.185	0.015	0	0	1.2	0.9	0	0.3	1.5
M3	MOX fuel	0.2	0.185	0.015	0	0	1.13	0.9	0	0.23	1.5
M4	MOX fuel	0.2	0.185	0.015	0	0	1.07	0.9	0	0.17	1.5
U1	Uranium fuel	0.2	0.2	0	0	0	0.2	0	0	0.2	1.5
U2	Uranium fuel	0.2	0.185	0.015	0	0	1.0	0.9	0	0.1	1.5
W	Water	0.2	0.17	0.03	0	0	1.1	1.1	0	0	0

pin 1	pin 2	pin 3	pin 4	pin 5	pin 6	pin 7	pin 8	pin 1	pin 2	pin 3	pin 4	pin 5	pin 6	pin 7	pin 8
M1	M1	M1	M1	M1	M1	M1	M1	U1	U1	U1	U1	U1	U1	U1	U1

Figure 1: Test 1, design of assemblies.

pin 1	pin 2	pin 3	pin 4	pin 5	pin 6	pin 7	pin 8	pin 1	pin 2	pin 3	pin 4	pin 5	pin 6	pin 7	pin 8
M2	M2	M2	M2	M2	M2	M2	M2	U2	U2	U2	U2	U2	U2	U2	U2

Figure 2: Test 2, design of assemblies.

pin 1	pin 2	pin 3	pin 4	pin 5	pin 6	pin 7	pin 8	pin 1	pin 2	pin 3	pin 4	pin 5	pin 6	pin 7	pin 8
M2	M2	M2	M2	M2	M2	M2	U2	U2	U2	U2	U2	U2	U2	U2	U2

Figure 3: Test 3, design of assemblies.

pin 1	pin 2	pin 3	pin 4	pin 5	pin 6	pin 7	pin 8	pin 1	pin 2	pin 3	pin 4	pin 5	pin 6	pin 7	pin 8
M2	M2	M2	M2	M2	M2	M3	M4	U2	U2	U2	U2	U2	U2	U2	U2

Figure 4: Test 4, design of assemblies.

pin 1	pin 2	pin 3	pin 4	pin 5	pin 6	pin 7	pin 8	pin 1	pin 2	pin 3	pin 4	pin 5	pin 6	pin 7	pin 8
M2	M2	M2	W	W	M2	M2	M2	U2	U2	U2	U2	U2	U2	U2	U2

Figure 5: Test 5, design of assemblies.

Table II. Test 1. CMFE-0 Method, Relative Difference in Pin-Cell Average Values.

Assembly	Group	Pin # 1	Pin # 2	Pin # 3	Pin # 4	Pin # 5	Pin # 6	Pin # 7	Pin # 8
MOX	1	$1\cdot10^{-4}$	$4\cdot10^{-4}$	$5\cdot10^{-4}$	$2\cdot10^{-4}$	$-4\cdot10^{-4}$	$-9\cdot10^{-4}$	$-4\cdot10^{-4}$	$5\cdot10^{-4}$
MOX	2	$3\cdot10^{-3}$	$4\cdot10^{-3}$	$4\cdot10^{-3}$	$4\cdot10^{-3}$	$4\cdot10^{-3}$	$1\cdot10^{-3}$	$-5\cdot10^{-3}$	$-1\cdot10^{-2}$
U	1	$6\cdot10^{-4}$	$6\cdot10^{-6}$	$8\cdot10^{-5}$	$4\cdot10^{-5}$	$-1\cdot10^{-4}$	$-2\cdot10^{-4}$	$-2\cdot10^{-4}$	$-1\cdot10^{-4}$
U	2	$1\cdot10^{-2}$	$4\cdot10^{-3}$	$-1\cdot10^{-3}$	$-3\cdot10^{-3}$	$-3\cdot10^{-3}$	$-2\cdot10^{-3}$	$-2\cdot10^{-3}$	$-3\cdot10^{-3}$

Table III. Test 1. CMFE-2 Method. Relative Difference in Pin-Cell Average Values.

Assembly	Group	Pin # 1	Pin # 2	Pin # 3	Pin # 4	Pin # 5	Pin # 6	Pin # 7	Pin # 8
MOX	1	$-7\cdot10^{-4}$	$3\cdot10^{-5}$	$6\cdot10^{-4}$	$6\cdot10^{-4}$	$4\cdot10^{-5}$	$-5\cdot10^{-4}$	$-4\cdot10^{-4}$	$3\cdot10^{-4}$
MOX	2	$-4\cdot10^{-3}$	$-2\cdot10^{-3}$	$7\cdot10^{-4}$	$3\cdot10^{-3}$	$4\cdot10^{-3}$	$4\cdot10^{-3}$	$-3\cdot10^{-4}$	$-5\cdot10^{-3}$
U	1	$-3\cdot10^{-4}$	$-4\cdot10^{-4}$	$2\cdot10^{-4}$	$5\cdot10^{-4}$	$5\cdot10^{-4}$	$2\cdot10^{-4}$	$-2\cdot10^{-4}$	$-4\cdot10^{-4}$
U	2	$-2\cdot10^{-2}$	$1\cdot10^{-2}$	$1\cdot10^{-2}$	$2\cdot10^{-3}$	$-6\cdot10^{-3}$	$-7\cdot10^{-3}$	$-2\cdot10^{-3}$	$4\cdot10^{-3}$

Table IV. Test 2. CMFE-0 Method. Relative Difference in Pin-Cell Average Values.

Assembly	Group	Pin # 1	Pin # 2	Pin # 3	Pin # 4	Pin # 5	Pin # 6	Pin # 7	Pin # 8
MOX	1	$5\cdot10^{-5}$	$5\cdot10^{-4}$	$6\cdot10^{-4}$	$1\cdot10^{-4}$	$-7\cdot10^{-4}$	$-1\cdot10^{-3}$	$-3\cdot10^{-4}$	$9\cdot10^{-4}$
MOX	2	$-2\cdot10^{-4}$	$-2\cdot10^{-4}$	$-2\cdot10^{-4}$	$-2\cdot10^{-4}$	$-1\cdot10^{-4}$	$-3\cdot10^{-4}$	$-1\cdot10^{-3}$	$2\cdot10^{-3}$
U	1	$5\cdot10^{-4}$	$-3\cdot10^{-4}$	$-8\cdot10^{-5}$	$7\cdot10^{-5}$	$-2\cdot10^{-5}$	$-1\cdot10^{-4}$	$-3\cdot10^{-5}$	$8\cdot10^{-5}$
U	2	$5\cdot10^{-4}$	$1\cdot10^{-4}$	$-7\cdot10^{-4}$	$-4\cdot10^{-4}$	$8\cdot10^{-5}$	$3\cdot10^{-4}$	$2\cdot10^{-4}$	$-5\cdot10^{-5}$

Table V. Test 2. CMFE-2 Method. Relative Difference in Pin-Cell Average Values.

Assembly	Group	Pin # 1	Pin # 2	Pin # 3	Pin # 4	Pin # 5	Pin # 6	Pin # 7	Pin # 8
MOX	1	$-7\cdot10^{-4}$	$1\cdot10^{-4}$	$8\cdot10^{-4}$	$6\cdot10^{-4}$	$-1\cdot10^{-4}$	$-7\cdot10^{-4}$	$-3\cdot10^{-4}$	$4\cdot10^{-4}$
MOX	2	$-3\cdot10^{-3}$	$-6\cdot10^{-4}$	$2\cdot10^{-3}$	$3\cdot10^{-3}$	$3\cdot10^{-3}$	$9\cdot10^{-4}$	$-2\cdot10^{-3}$	$-2\cdot10^{-3}$
U	1	$-2\cdot10^{-4}$	$-7\cdot10^{-4}$	$1\cdot10^{-4}$	$6\cdot10^{-4}$	$6\cdot10^{-4}$	$2\cdot10^{-4}$	$-2\cdot10^{-4}$	$-5\cdot10^{-4}$
U	2	$-1\cdot10^{-3}$	$-2\cdot10^{-4}$	$4\cdot10^{-5}$	$8\cdot10^{-4}$	$1\cdot10^{-3}$	$8\cdot10^{-4}$	$-2\cdot10^{-4}$	$1\cdot10^{-3}$

Table VI. Test 3. CMFE-0 Method. Relative Difference in Pin-Cell Average Values.

Assembly	Group	Pin # 1	Pin # 2	Pin # 3	Pin # 4	Pin # 5	Pin # 6	Pin # 7	Pin # 8
MOX	1	$4\cdot10^{-3}$	$5\cdot10^{-3}$	$5\cdot10^{-3}$	$4\cdot10^{-3}$	$2\cdot10^{-3}$	$5\cdot10^{-4}$	$-1\cdot10^{-3}$	$-2\cdot10^{-2}$
MOX	2	$-1\cdot10^{-1}$	$-1\cdot10^{-1}$	$-1\cdot10^{-1}$	$-1\cdot10^{-1}$	$-9\cdot10^{-2}$	$-2\cdot10^{-2}$	$1\cdot10^{-1}$	$3\cdot10^{-1}$
U	1	$-4\cdot10^{-4}$	$-3\cdot10^{-4}$	$6\cdot10^{-5}$	$2\cdot10^{-4}$	$2\cdot10^{-4}$	$1\cdot10^{-4}$	$9\cdot10^{-5}$	$7\cdot10^{-5}$
U	2	$5\cdot10^{-4}$	$-3\cdot10^{-4}$	$-4\cdot10^{-4}$	$-2\cdot10^{-4}$	$4\cdot10^{-5}$	$2\cdot10^{-4}$	$1\cdot10^{-4}$	$5\cdot10^{-5}$

Table VII. Test 3. CMFE-2 Method. Relative Difference in Pin-Cell Average Values.

Assembly	Group	Pin # 1	Pin # 2	Pin # 3	Pin # 4	Pin # 5	Pin # 6	Pin # 7	Pin # 8
MOX	1	$1\cdot10^{-3}$	$-9\cdot10^{-5}$	$-2\cdot10^{-3}$	$-2\cdot10^{-3}$	$-1\cdot10^{-3}$	$3\cdot10^{-3}$	$8\cdot10^{-3}$	$-7\cdot10^{-3}$
MOX	2	$-5\cdot10^{-2}$	$1\cdot10^{-2}$	$6\cdot10^{-2}$	$5\cdot10^{-2}$	$2\cdot10^{-3}$	$-6\cdot10^{-2}$	$-6\cdot10^{-2}$	$5\cdot10^{-2}$
U	1	$-4\cdot10^{-4}$	$-2\cdot10^{-4}$	$3\cdot10^{-4}$	$5\cdot10^{-4}$	$3\cdot10^{-4}$	$1\cdot10^{-4}$	$-2\cdot10^{-4}$	$-3\cdot10^{-4}$
U	2	$-1\cdot10^{-3}$	$-7\cdot10^{-4}$	$2\cdot10^{-4}$	$1\cdot10^{-3}$	$1\cdot10^{-3}$	$8\cdot10^{-4}$	$-3\cdot10^{-4}$	$-1\cdot10^{-3}$

Table VIII. Test 4. CMFE-0 Method. Relative Difference in Pin-Cell Average Values.

Assembly	Group	Pin # 1	Pin # 2	Pin # 3	Pin # 4	Pin # 5	Pin # 6	Pin # 7	Pin # 8
MOX	1	$3\cdot10^{-3}$	$2\cdot10^{-3}$	$2\cdot10^{-3}$	$2\cdot10^{-3}$	$2\cdot10^{-3}$	$2\cdot10^{-3}$	$-9\cdot10^{-3}$	$-5\cdot10^{-3}$
MOX	2	$-1\cdot10^{-1}$	$-1\cdot10^{-1}$	$-1\cdot10^{-1}$	$-8\cdot10^{-2}$	$-5\cdot10^{-2}$	$3\cdot10^{-2}$	$1\cdot10^{-1}$	$1\cdot10^{-1}$
U	1	$2\cdot10^{-4}$	$-3\cdot10^{-4}$	$-3\cdot10^{-5}$	$1\cdot10^{-4}$	$4\cdot10^{-5}$	$-4\cdot10^{-5}$	$4\cdot10^{-6}$	$7\cdot10^{-5}$
U	2	$2\cdot10^{-4}$	$9\cdot10^{-5}$	$-5\cdot10^{-4}$	$-3\cdot10^{-4}$	$6\cdot10^{-5}$	$3\cdot10^{-4}$	$2\cdot10^{-4}$	$-1\cdot10^{-5}$

Table IX. Test 4. CMFE-2 Method. Relative Difference in Pin-Cell Average Values.

Assembly	Group	Pin # 1	Pin # 2	Pin # 3	Pin # 4	Pin # 5	Pin # 6	Pin # 7	Pin # 8
MOX	1	$5\cdot10^{-4}$	$-6\cdot10^{-4}$	$-1\cdot10^{-3}$	$-5\cdot10^{-4}$	$2\cdot10^{-3}$	$4\cdot10^{-3}$	$-5\cdot10^{-3}$	$1\cdot10^{-3}$
MOX	2	$-1\cdot10^{-2}$	$8\cdot10^{-3}$	$2\cdot10^{-2}$	$3\cdot10^{-3}$	$-2\cdot10^{-2}$	$-2\cdot10^{-2}$	$3\cdot10^{-2}$	$-1\cdot10^{-2}$
U	1	$-3\cdot10^{-4}$	$-5\cdot10^{-4}$	$2\cdot10^{-4}$	$6\cdot10^{-4}$	$5\cdot10^{-4}$	$2\cdot10^{-4}$	$-2\cdot10^{-4}$	$-4\cdot10^{-4}$
U	2	$-1\cdot10^{-3}$	$-3\cdot10^{-4}$	$1\cdot10^{-4}$	$9\cdot10^{-4}$	$1\cdot10^{-3}$	$8\cdot10^{-4}$	$-3\cdot10^{-4}$	$-1\cdot10^{-3}$

Table X. Test 5. CMFE-0 Method. Relative Difference in Pin-Cell Average Values.

Assembly	Group	Pin # 1	Pin # 2	Pin # 3	Pin # 4	Pin # 5	Pin # 6	Pin # 7	Pin # 8
MOX	1	$1{\cdot}10^{-2}$	$2{\cdot}10^{-2}$	$1{\cdot}10^{-2}$	$-6{\cdot}10^{-2}$	$-6{\cdot}10^{-2}$	$1{\cdot}10^{-2}$	$2{\cdot}10^{-2}$	$2{\cdot}10^{-2}$
MOX	2	$-4{\cdot}10^{-1}$	$-3{\cdot}10^{-1}$	$3{\cdot}10^{-2}$	$3{\cdot}10^{-1}$	$3{\cdot}10^{-1}$	$2{\cdot}10^{-3}$	$-3{\cdot}10^{-1}$	$-4{\cdot}10^{-1}$
U	1	$1{\cdot}10^{-3}$	$-3{\cdot}10^{-4}$	$-2{\cdot}10^{-4}$	$-9{\cdot}10^{-5}$	$-2{\cdot}10^{-4}$	$-3{\cdot}10^{-4}$	$-1{\cdot}10^{-4}$	$4{\cdot}10^{-5}$
U	2	$3{\cdot}10^{-4}$	$4{\cdot}10^{-4}$	$-5{\cdot}10^{-4}$	$-4{\cdot}10^{-4}$	$4{\cdot}10^{-6}$	$2{\cdot}10^{-4}$	$1{\cdot}10^{-4}$	$-1{\cdot}10^{-4}$

Table XI. Test 5. CMFE-2 Method. Relative Difference in Pin-Cell Average Values.

Assembly	Group	Pin # 1	Pin # 2	Pin # 3	Pin # 4	Pin # 5	Pin # 6	Pin # 7	Pin # 8
MOX	1	$-9{\cdot}10^{-3}$	$1{\cdot}10^{-2}$	$3{\cdot}10^{-2}$	$-3{\cdot}10^{-2}$	$-3{\cdot}10^{-2}$	$3{\cdot}10^{-2}$	$1{\cdot}10^{-2}$	$-8{\cdot}10^{-3}$
MOX	2	$1{\cdot}10^{-1}$	$-1{\cdot}10^{-1}$	$-2{\cdot}10^{-2}$	$1{\cdot}10^{-1}$	$1{\cdot}10^{-1}$	$-1{\cdot}10^{-1}$	$-1{\cdot}10^{-1}$	$-7{\cdot}10^{-2}$
U	1	$-1{\cdot}10^{-4}$	$-8{\cdot}10^{-4}$	$5{\cdot}10^{-5}$	$6{\cdot}10^{-4}$	$6{\cdot}10^{-4}$	$3{\cdot}10^{-4}$	$-2{\cdot}10^{-4}$	$-5{\cdot}10^{-4}$
U	2	$-1{\cdot}10^{-3}$	$-1{\cdot}10^{-4}$	$6{\cdot}10^{-5}$	$8{\cdot}10^{-4}$	$1{\cdot}10^{-3}$	$8{\cdot}10^{-4}$	$-2{\cdot}10^{-4}$	$-1{\cdot}10^{-3}$

Table XII. Maximum Relative Differences in Pin-Cell Average Values in MOX Assemblies.

Test	CMFE-0		CMFE-2	
	fast group	thermal group	fast group	thermal group
1	$5{\cdot}10^{-4}$	$1{\cdot}10^{-2}$	$7{\cdot}10^{-4}$	$5{\cdot}10^{-3}$
2	$1{\cdot}10^{-3}$	$2{\cdot}10^{-3}$	$8{\cdot}10^{-4}$	$5{\cdot}10^{-3}$
3	$2{\cdot}10^{-2}$	$3{\cdot}10^{-1}$	$8{\cdot}10^{-3}$	$6{\cdot}10^{-2}$
4	$9{\cdot}10^{-3}$	$1{\cdot}10^{-1}$	$5{\cdot}10^{-3}$	$3{\cdot}10^{-2}$
5	$6{\cdot}10^{-2}$	$4{\cdot}10^{-1}$	$3{\cdot}10^{-2}$	$1{\cdot}10^{-1}$

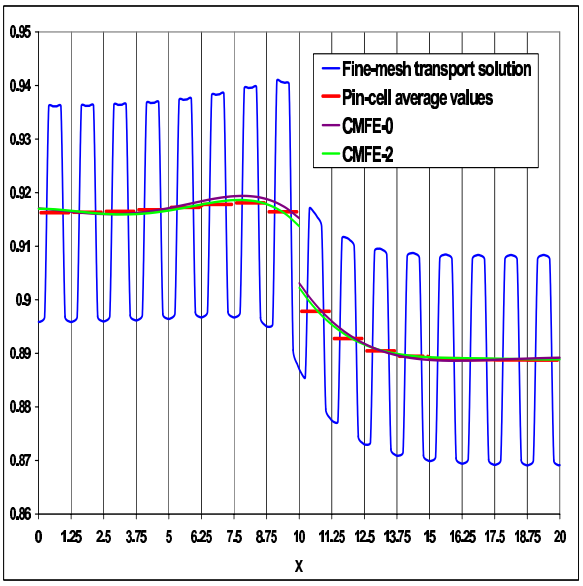

Figure 6. Test 1. The fast scalar flux versus position.

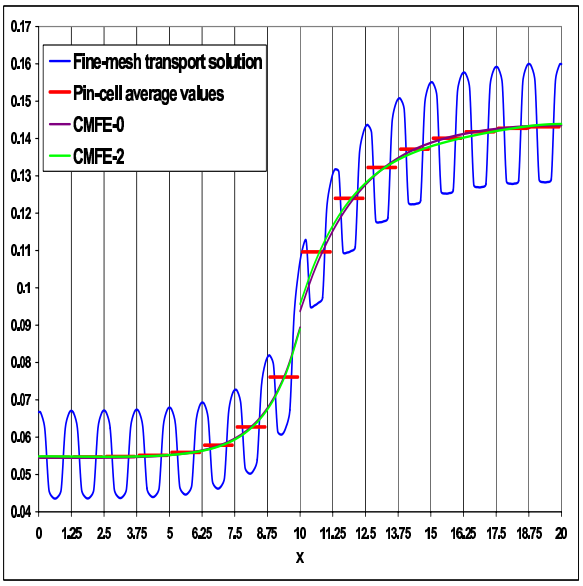

Figure 7. Test 1. The thermal scalar flux versus position.

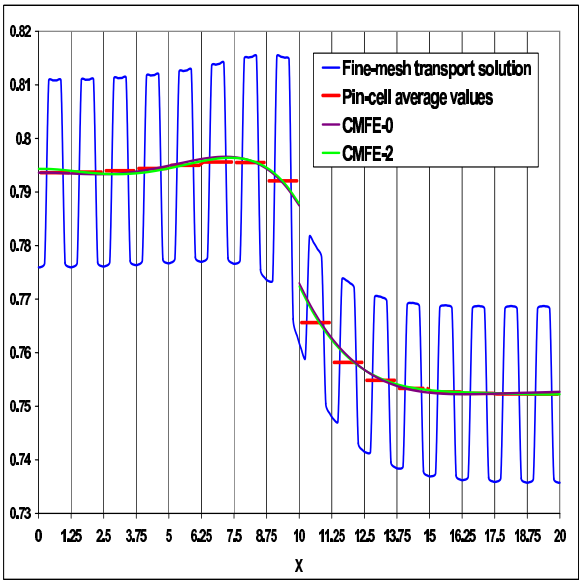

Figure 8. Test 2. The fast scalar flux versus position.

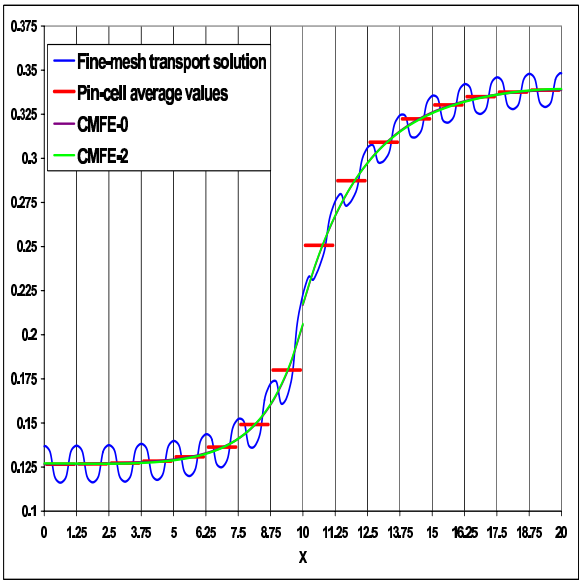

Figure 9. Test 2. The thermal scalar flux versus position.

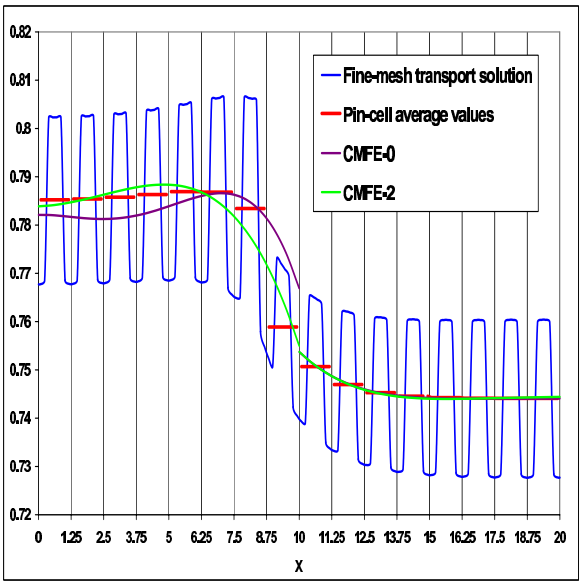

Figure 10. Test 3. The fast scalar flux versus position.

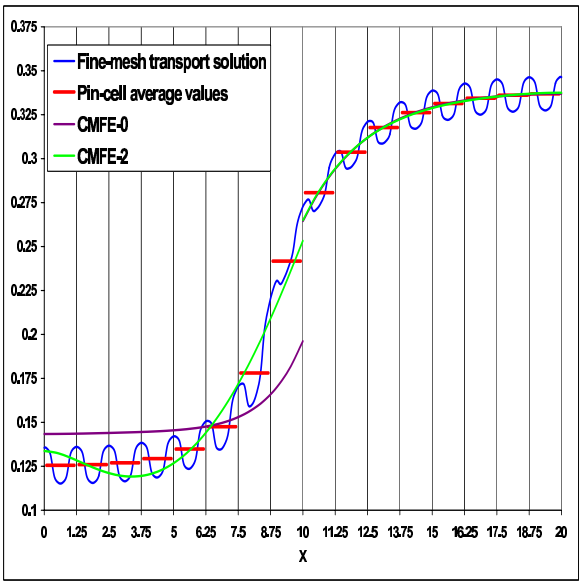

Figure 11. Test 3. The thermal scalar flux versus position.

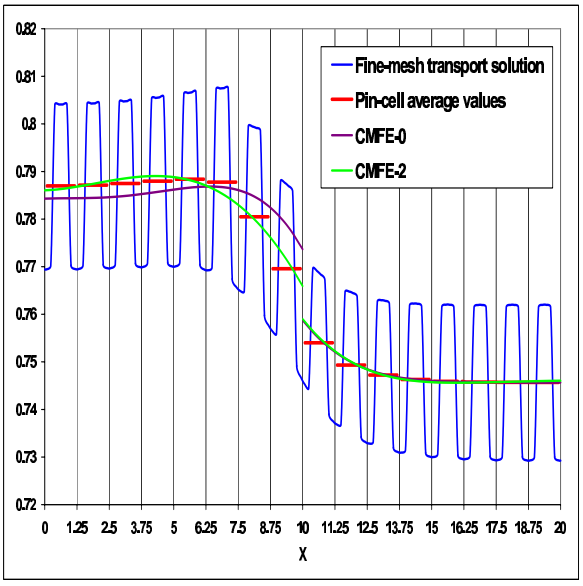

Figure 12. Test 4. The fast scalar flux versus position.

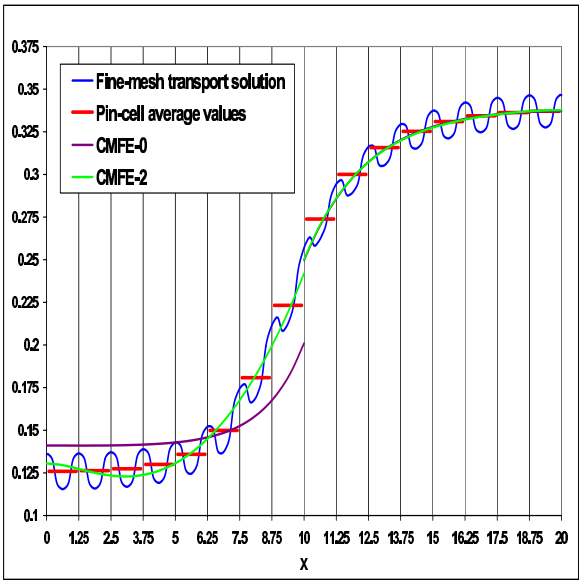

Figure 13. Test 4. The thermal scalar flux versus position.

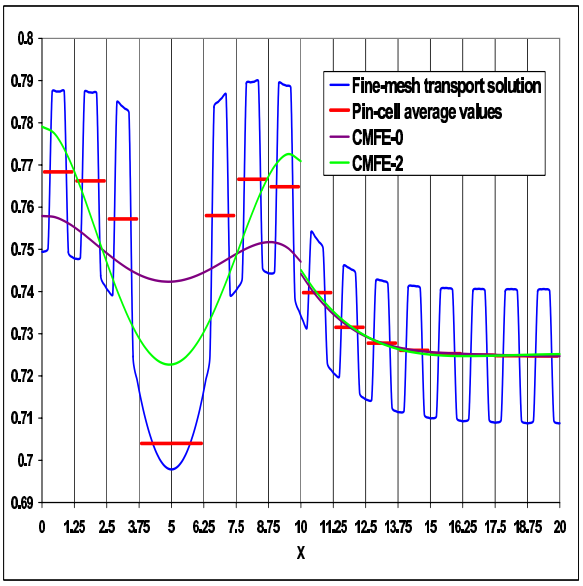

Figure 14. Test 5. The fast scalar flux versus position.

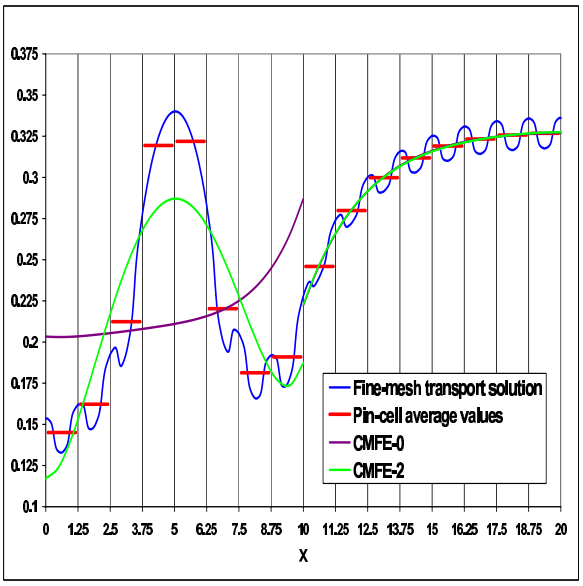

Figure 15. Test 5. The thermal scalar flux versus position.

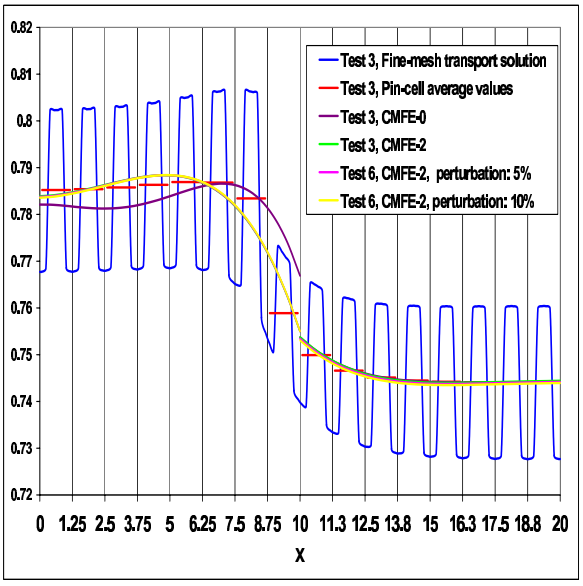

Figure 16. Test 6. The fast scalar flux versus position.

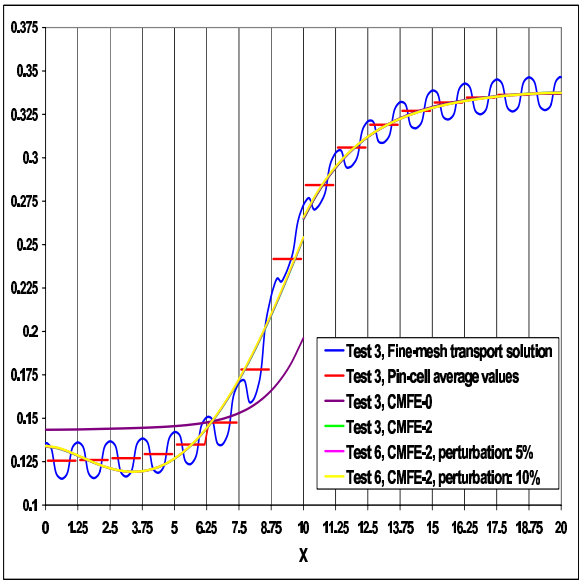

Figure 17. Test 6. The thermal scalar flux versus position .

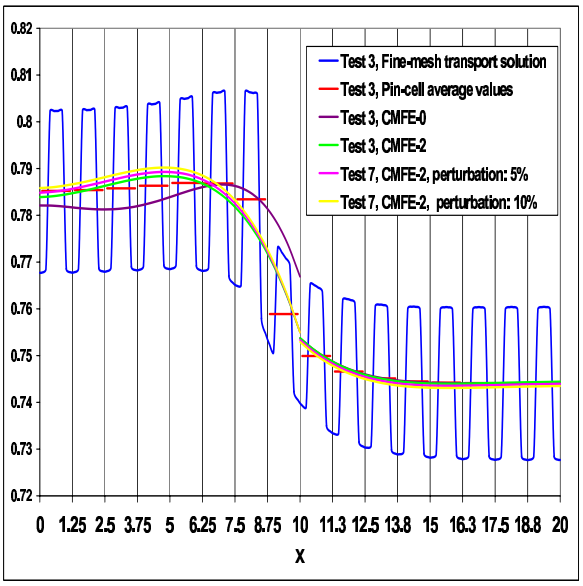

Figure 18. Test 7. The fast scalar flux versus position.

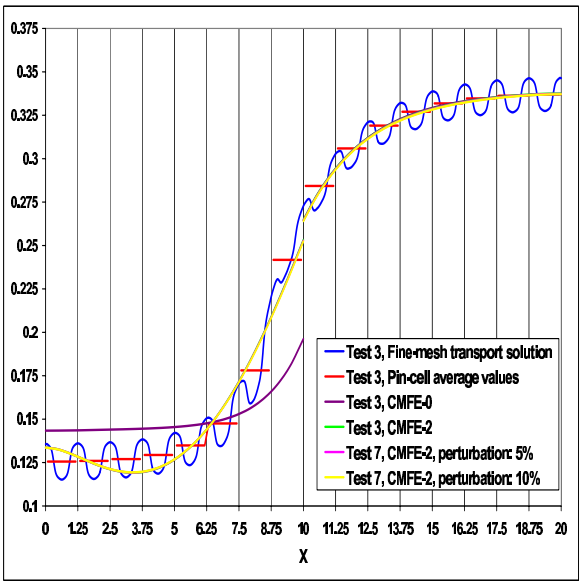

Figure 19. Test 7. The thermal scalar flux versus position.

We have analyzed the developed methods on a set of test problems that simulate the interaction of MOX and uranium assemblies. These tests included assemblies with enrichment variations, and water holes that introduce within-assembly flux variations. In spite of this the CMFE-2 method is able to generate solution that mimic accurately the large-scale behavior of the transport solution within assembly.

The proposed methodology can be extended to multidimensional geometries, multigroup case, finite-element methods based on higher order expansions of the coarse-mesh scalar flux that creates an option of preserving more spatial moments of the fine-mesh transport solution over coarse cells. The developed method is a part of a new methodology for reactor core calculations, and this method will be coupled with other pieces of this methodology, including usage of group data obtained by means of single-assembly calculations that use efficient albedo boundary conditions. Another important issue is possibility of improvement of pin-power reconstruction using the discretization methods that preserve extra spatial moments of the fine-mesh transport solution within assembly. We are working now on such extensions.

ACKNOWLEDGEMENTS

The author thanks Marvin Adams, Todd Palmer and Kord Simth for many helpful discussions. This work was supported by Nuclear Energy Research Initiative (NERI) Program of the US Department of Energy under grant No. DE-FG03-99SF21922.

REFERENCES

[1] D.Y. Anistratov and M.L. Adams, “Consistent Coarse-Mesh Discretization of the Low-Order Equations of the Quasidiffusion Method,” *Trans. Am. Nucl. Soc.*, **83**, 250-251 (2000).

[2] K. T. Clarno and M. L. Adams, "Improved Boundary Conditions for Assembly-Level Transport Codes," *Int. Conf. on the New Frontiers of Nuclear Technology: Reactor Physics, Safety and High-Performance Computing (PHYSOR 2002)*, Seoul, Korea, Oct. 7-10 (2002).

[3] R. Nes and T. S. Palmer, "An Advanced Nodal Discretization for the Quasi-Diffusion Low-Order Equations," *Int. Conf. on the New Frontiers of Nuclear Technology: Reactor Physics, Safety and High-Performance Computing (PHYSOR 2002)*, Seoul, Korea, Oct. 7-10 (2002).

[4] D. Y. Anistratov, "Homogenization Methodology for the Low-Order Equations of the Quasidiffusion Method," *Int. Conf. on the New Frontiers of Nuclear Technology: Reactor Physics, Safety and High-Performance Computing (PHYSOR 2002)*, Seoul, Korea, Oct. 7-10 (2002).

[5] H. Hikaru, D. Y. Anistratov, and M. L. Adams, "Splitting Method for Solving the Coarse-Mesh Discretized Low-Order Quasidiffusion Equations," this proceedings (2003).

[6] K. T. Clarno and M. L. Adams, "Capturing the Effects of Unlike Neighbors in Single-Assembly Calculations," this proceedings (2003).

[7] V.Ya. Gol'din, "A Quasidiffusion Method for Solving the Kinetic Equation," *USSR Comp. Math. and Math. Phys.* **4**, 136-149 (1964).

[8] N. N. Aksenov and V. Ya. Gol'din, "Computation of the Two-Dimensional Stationary Equation of Neutron Transfer by the Quasi-Diffusion Method," *USSR Comp. Math. and Math. Phys.*, **19**, No. 5, 263-266 (1979).

[9] V. Ya. Gol'din, "On Mathematical Modeling of Problems of Non-Equilibrium Transfer in Physical Systems," in *Modern Problems of Mathematical Physics and Computational Mathematics*, Nauka, Moscow, 113-127 (1982) (in Russian).

[10] K. S. Smith, "Assembly Homogenization Techniques for Light Water Reactor Analysis," *Progress in Nuclear Energy*, **17**, 303-335 (1986).

[11] D. Y. Anistratov and V. Ya. Gol'din, "Solving the Multigroup Transport Equation by the Quasidiffusion Method," *Preprint of the Keldysh Institute for Applied Mathematics*, the USSR Academy of Sciences, No. 128 (1986) (in Russian).

[12] E.N.Aristova, V.Ya. Gol'din, and A.V.Kolpakov, "Multidimensional Calculations of Radiation Transport by Nonlinear Quasi-Diffusion Method," *Proceeding of ANS International Conference on Mathematics and Computation, Reactor Physics and Environmental Analysis in Nuclear Applications*, Sept. 27-30, 1999, Madrid, Spain, 667-676 (1999).

[13] D.Y. Anistratov and V.Ya. Gol'din, "Nonlinear Methods for Solving Particle Transport Problems," *Transport Theory Statist. Phys.* **22** 42–77 (1993).

[14] K. S. Smith, *private communication*.